Indian Journal of Pure & Applied Physics
Vol. 58, March 2020, pp. 157-163

Spectroscopic properties of Sm^{3+} and CdS co-doped in sol-gel silica glass

Md Uzair Khan, A L Fanai & S Rai*

Laser and Photonics Laboratory, Department of Physics,
Mizoram University, Aizawl 796 004, India

Received 30 April 2019; accepted 10 January 2020

Sm^{3+}- doped silica glass co-doped with CdS nanoparticles have been prepared by sol-gel method. FTIR spectra of the samples at different annealing temperatures show the gradual removal of hydroxyl group. XRD pattern shows crystalline nature of the silica host along with CdS peak. The optical absorption and fluorescence properties have been investigated using Judd-Ofelt theory. The Judd-Ofelt intensity parameters have been obtained from the absorption spectrum following the trend $\Omega_2 > \Omega_4 > \Omega_6$ and the large value of Ω_2 indicates covalency of the rare earth bonding. Under excitation with 370 nm, photoluminescence peaks have been observed in the green, yellow, orange and red region as a result of radiative relaxation from the $^4G_{5/2}$ state.

Keywords: Sol-gel, Samarium, CdS, Judd-Ofelt, Photoluminescence, Radiative-relaxation.

1 Introduction

Trivalent rare earth $(RE)^{3+}$ ions are popular doping ions for various types of glasses and laser materials[1,2]. Rare earth (RE) ions are chosen because of their high quantum efficiencies and their narrow emission bands, which results from transition within the internal 4f electronic shells. Rare earth (RE) ions can easily be incorporated in large quantities in a silica gel host by the sol-gel process[3-6]. The sol-gel process is a room temperature method for the synthesis of inorganic hosts that permits a homogeneous doping in a silica matrix[7]. Trivalent samarium (Sm^{3+}) ion exhibits a strong luminescence in the visible spectral regions[8]. Recently, a great deal of attention has been devoted to the visible wavelength range for use in several applications, including optical data storage, optical amplifier, sensor and laser material processing. There have a relationship between the active ions and the host glasses. One important point is that to achieve strong up-conversion luminescence the glass host with low phonon energy can reduce the non-radiative loss due to the multi phonon relaxation[9]. CdS is an important II-VI direct band gap semiconductor with different applications in optoelectronics, photo catalysts, solar cell, nonlinear optical materials, Sensors, address decoders, and electrically driven lasers[10-16]. Bulk CdS has hexagonal wurtzite-type structure, melting point 1600 °C and band gap Eg = 2.42 eV at room temperature[17-19]. Since, CdS has 2.42 eV (515 nm) band gap, so it is most promising candidate among II-VI compounds for detecting visible radiation. Eu^{3+} ion doped in CdS nanoparticles and silica xero gels was discussed by Hayakawa *et al*.[20,21] and CdS quantum dots in ZrO_2 films together with lanthanide ions (Eu^{3+} and Tb^{3+}) was discussed by Reisfeld *et al*.[22].

In the present work we discuss the synthesis of Sm^{3+} ions in silica xero gels co-doped with CdS nanoparticle. We studied XRD, absorption, PL spectra, the FTIR spectra of Sm^{3+} ion in sol-gel silica glass at different annealing temperatures; optical properties are studied from the absorption spectra and J-O intensity parameters, radiative properties of the glasses, transition probability, spontaneous emission probabilities, the stimulated emission cross section and the branching ratios are determined in the visible region using Judd-Ofelt analysis. The calculations were done for the sample with 7 % Sm and 1 % CdS concentrations.

2 Experimental Details

2.1 Sample preparation

Sm^{3+}-doped silica glasses were prepared by sol-gel process using a two-step hydrolysis process[23], using tetraethylorthosilicate (TEOS) and $Sm(NO_3)_3.6H_2O$ as starting materials. First, 1.5 ml of TEOS is used for hydrolysis at room temperature for 30 min in a mix solution with deionized H_2O, C_2H_5OH, conc. HNO_3 maintaining the molar ratio 1:5.5:3.5:0.1 of $TEOS:H_2O:C_2H_5OH:HNO_3$ and added with

*Corresponding author (E-mail: srai.rai677@gmail.com)

appropriate amounts of $Sm(NO_3)_3.6H_2O$ which was stirred for 1 h.

Secondly, $CdN_2O_6.4H_2O$ is mixed with $SC(NH_2)_2$ (thiourea), ethanol solution, which stirring for 1 h using a magnetic stirrer to form a sol. Now combining both the mixture stirred for 4 h. After rigorous stirring the sol is poured in a plastic container which is sealed to prevent evaporation and left for a few days at room temperature to form a stiff gel. In the cover of the container some pin holes are made for slow evaporation and then left for three to four weeks. Evaporation should be very slow; otherwise non-uniform shrinkage can lead to deformed and cracked the sample. The gels were dried for slowly heating to 110°C by an electric muffle furnace to form disc shaped samples. The refractive index was obtained by measuring the Brewster angle. The disc shaped samples have thickness 2 mm and diameter 16 mm, density 2.08 g/cm^3 and refractive index 1.54.

2.2 Experimental set-up

The absorption spectra were recorded in the UV-visible region using iHR320 imaging (HORIBA). The PL spectra of the prepared sample were recorded using iHR320 imaging spectrometer using Syner JY^{TM} software from Horiba Scientific fully integrated data acquisition and data analysis for spectroscopic systems and the excitation source was 370 nm LED. FTIR spectra were recorded by IRAffinity-1S (SHIMADZU). All the spectra were recorded at room temperature.

3 Results

3.1 FTIR analysis

The FT-IR spectrum of the Sm^{3+} doped with CdS and sol-gel silica glass at different temperature is shown in Fig. 1. Here Si-OH group comes from the hydrolysis of TEOS, through polycondensation reaction. At the gel stage sol-gel samples have lot of water with other organics. On heating the prepared sample by muffle furnace the compounds gradually escape from the matrix and form a rigid glassy network. The bands located at 552 cm^{-1}, 787 cm^{-1} and 1042 cm^{-1} are for Si-OH groups forming Si-O-Si bonds in cyclic structure. In the gels heated to 350 °C, the presence of Si-O free broken bond at 954 cm^{-1} has been detected. The band at 954 cm^{-1} is a weak band for the polymerization process of Si-OH groups. Another four bands appeared at about 1327 cm^{-1}, 1631 cm^{-1}, 2367 cm^{-1} and 3367 cm^{-1}. Here bands at 1631 cm^{-1} and 3367 cm^{-1} are due to water molecules.

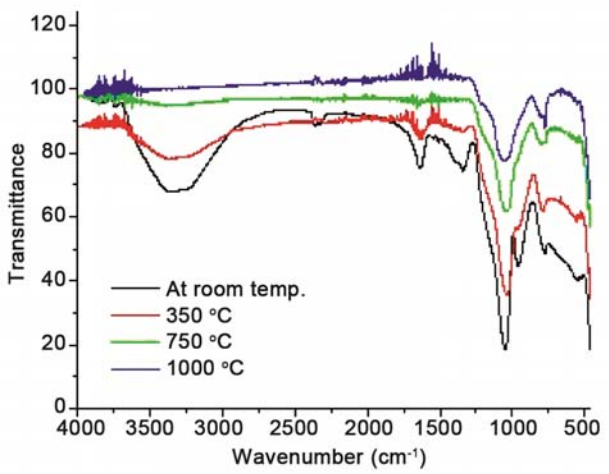

Fig. 1 — FT-IR Spectra of Sm^{3+} doped with CdS in silica glass at different temperatures.

In gel derived silica glasses of broken Si-O bonds in the silica network, from which we get a peak at 856 cm^{-1} in the IR spectra. After forming the Sm-O-Si bond, a new band is produced by new silicate anions at 954 cm^{-1}. By the breaking of Si-O-Si bonds a non-bridging oxygen (NBO) is formed for samarium. The band due to the -OH stretching vibration around 3367 cm^{-1} that may present and the corresponding OH bending presence of adsorbed water at 1631 cm^{-1}. The gradual disappearance of the band centered at 3367 cm^{-1} with increasing temperature indicates the gradual removal of –OH as a result of evaporation.

3.2 Absorption and PL spectra

The absorption spectrum and emission spectrum of CdS doped in silica xerogel are shown in Fig. 2 (a) and (b). The size dependent properties of CdS nanoparticle arise from quantum confinement as a direct consequence of the crystallite size. The photo generated carriers, i.e., electrons and holes, feel the spatial confinement, as a consequence of the energy level shift to higher energy. This leads to an increase in the band gap.

The absorption spectrum of CdS doped in silica xerogel is shown in Fig. 2(c). The size dependent properties of CdS nanoparticle arise from quantum confinement as a direct consequence of the crystallite size. The photo generated carriers, i.e., electrons and holes, feel the spatial confinement, as a consequence of the energy level shift to higher energy. This leads to an increase in the band gap (2.975 eV) as compared to that of bulk CdS (2.42 eV).

Figure 3 shows the absorption spectrum of the sample (7 mol % Sm, 1 mol % CdS) heated to 110 °C.

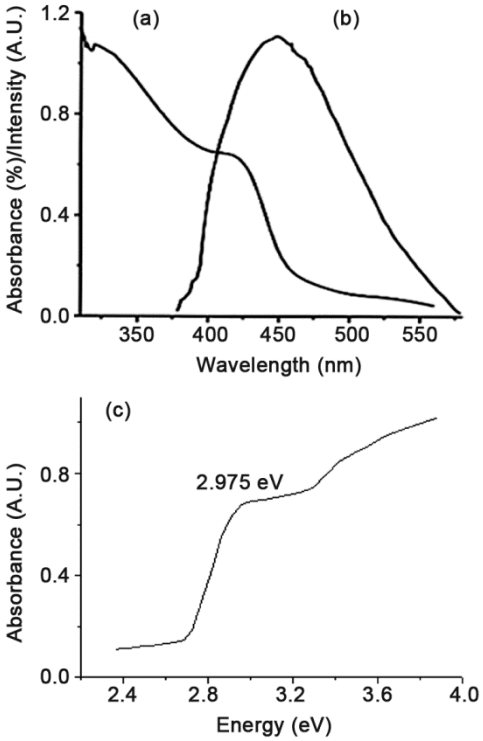

Fig. 2 — (a) Optical absorption, (b) PL spectra of CdS alone doped glass, and (c) optical absorption and band gap of CdS alone doped glass.

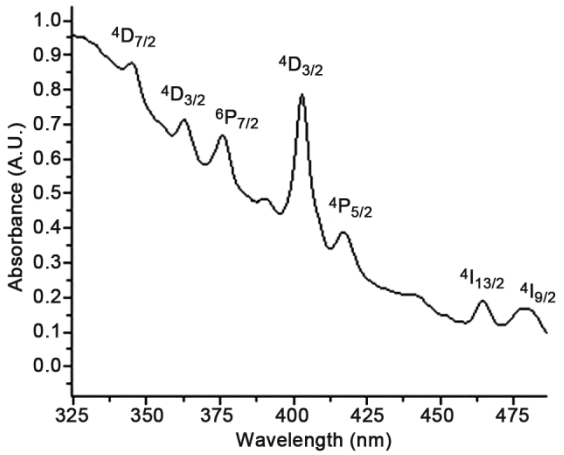

Fig. 3 — Absorption spectra of 7 % Sm and 1 % CdS co-doped sample.

A series of sharp series absorption bands present between 325-475 nm centered at the band assignments are also indicated in Fig. 4 which corresponds to the typical f-f transition of Sm^{3+} ions. The observed transitions are labeled as $^6H_{5/2} \rightarrow {}^4D_{7/2}$ (346 nm), $^6H_{5/2} \rightarrow {}^4D_{3/2}$ (362 nm), $^6H_{5/2} \rightarrow {}^6P_{7/2}$ (375 nm), $^6H_{5/2} \rightarrow {}^6P_{3/2}$ (403 nm), $^6H_{5/2} \rightarrow {}^6P_{5/2}$ (416 nm), $^6H_{5/2} \rightarrow {}^4I_{13/2}$ (464 nm) and $^6H_{5/2} \rightarrow {}^4I_{9/2}$ (478 nm).

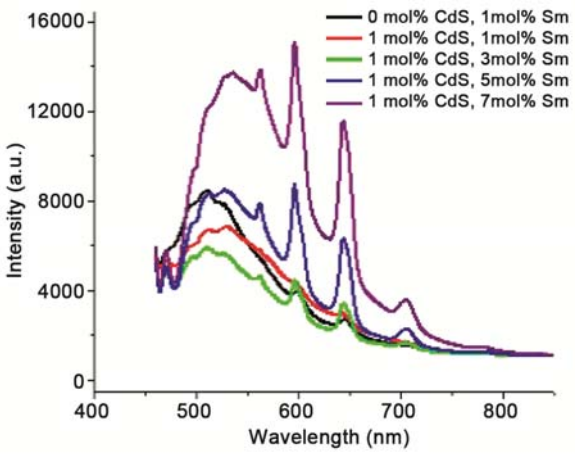

Fig. 4 — PL spectra of Sm^{3+} doped SiO_2 glasses with CdS concentrations.

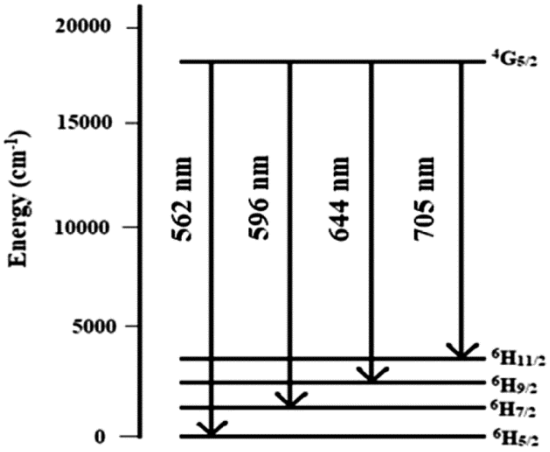

Fig. 5 — PL mechanism of Sm^{3+} ion in visible range.

The photoluminescence spectrum in the range of 400-850 nm is shown in Fig. 4. The emission spectra exhibit four emission bands centered at 562 nm, 596 nm, 644 nm and 705 nm. The emission peaks assigned to the transition of $^4G_{5/2} \rightarrow {}^6H_{5/2}$, $^4G_{5/2} \rightarrow {}^6H_{7/2}$, $^4G_{5/2} \rightarrow {}^6H_{9/2}$ and $^4G_{5/2} \rightarrow {}^6H_{11/2}$, respectively transitions of the Sm^{3+} ions. The $^4G_{5/2} \rightarrow {}^6H_{7/2}$ transition is the strongest while the $^4G_{5/2} \rightarrow {}^6H_{11/2}$ is the weakest transition in the present study. From these emission bands a possible color could be expected as moderate green, moderate yellow, intense orange and feeble red. Figure 5 shows the energy level diagram of Sm^{3+} for silica glass. $^4G_{5/2} \rightarrow {}^6H_{5/2, 7/2}$ transitions are magnetic dipole allowed transitions. But for the transition $^4G_{5/2} \rightarrow {}^6H_{7/2}$, electric dipole (ED) is dominated with the selection rule $\Delta J = \pm 1$ despite its magnetic dipole (MD) allowed transition properties, so it is partly a MD and partly an ED in nature.

The $^4G_{5/2} \rightarrow {}^6H_{9/2,\ 11/2}$ transitions are purely electric dipole transitions. The intensity ratio of ED to MD transitions is used to determine the symmetry of local environment of the trivalent ions. Greater the intensity of ED transition, the more asymmetry in nature. Comparing the intensity of the transition $^4G_{5/2} \rightarrow {}^6H_{5/2}$ and $^4G_{5/2} \rightarrow {}^6H_{9/2}$ it is observed that the ED transition is dominant over the MD transition which shows the asymmetry of the Sm^{3+} ion sites in the glass. In Fig. 4, it appears as if the intensity of the $^4G_{5/2} \rightarrow {}^6H_{5/2}$ transition at 562 nm is greater than that of the $^4G_{5/2} \rightarrow {}^6H_{9/2}$ transition at 644 nm, but this is due to the broad emission in the background due to the CdS. Subtracting this background it is clear that the $^4G_{5/2} \rightarrow {}^6H_{9/2}$ ED transition dominates over the $^4G_{5/2} \rightarrow {}^6H_{5/2}$ MD transition.

4 Discussions

4.1 Effective mass approximation (EMA)

To determine the particle size of CdS nanoparticles we use EMA formula to estimate the average particle size. In the optical absorption for creating an electron and hole for the photon energy is larger than band gap of semiconductor. The binding energy of the exciton is influenced by the presence of electrons in the solid which screen the hole. Nanoparticle has a Bohr radius with blue shift in the excitation energy is called quantum size effect is due to broadening of band gap with finite size. To explain the effective mass approximation formula (EMA), Brus[24] explain the theory of blue shift, gives energy E(R) as a function of nanoparticle radius R, as follows:

$$E(R) = E_0 + \frac{\hbar\pi^2}{2R^2}\left(\frac{1}{m_e} + \frac{1}{m_h}\right) - \frac{1.8e^2}{\epsilon R} + \frac{e^2}{R}\overline{\sum_{n=1}^{\infty} \alpha_n \left(\frac{S}{R}\right)^{2n}} \quad \ldots (1)$$

Where, R is the cluster radius, E_0 is the band gap, m_e is the effective mass of electrons, m_h is the effective mass of holes and e is the electronic charge. ϵ is the dielectric constant of the medium, α_n is the function of dielectric constant and S is the electron-hole separation. The second term of Eq. (1) represents quantum localization energy. The third term represents Coulomb potential energy and the fourth term represents polarization energy. For CdS cluster the eigen values of lowest excited states is located is no longer parabolic for the energy band so the curvature of lowest conduction band and highest valance band decreases with decreasing cluster size. From Eq. (1), the second and third term can be omitted because of smaller value of Coulomb potential and polarization energy, compared to electron-hole confinement kinetic energy. So, Eq. (1) can be written as:

$$E(R) = E_0 + \frac{\hbar\pi^2}{2R^2}\left(\frac{1}{m_e} + \frac{1}{m_h}\right) \quad \ldots (2)$$

Where, E(R) =2.975 eV, E_0= 2.42 eV, m_e= 0.21m_0, m_h= 0.80m_0, m_0= 9.109 $\times 10^{-31}$ kg is the free electron mass. The diameter of CdS nanoparticle was found 4.01 nm by using the EMA formula. For smaller diameter of a particle, surface area would be larger which confirms stronger contribution of the defect related luminescence emission.

4.2 PL Spectra of CdS nanoparticle

With excitation wavelength 370 nm is shown in Fig. 2(b). The PL spectra of CdS nanoparticle give the size of CdS nanoparticle. The blue shift of the PL spectra of CdS nanoparticle is observed. The PL peak shift from 450-550 nm. This is expected in few of the increased surface area of the nanoparticle and probability of emission from the defect centers. The surface defects play key role in the determining the luminescence property. In the bulk crystalline material charge carriers can be trapped at dopant ions. However, the nanoparticles this traps are most likely to be located.

4.3 XRD analysis

Figure 6 shows X-Ray powder diffraction pattern of CdS nanoparticles in SiO_2 sol-gel at 1000 °C. The broad peak centered on 2θ = 22° is characteristic of the amorphous silica glass. The sharp peak at 2θ = 26.6° is due to the (002) plane of CdS[12]. The size

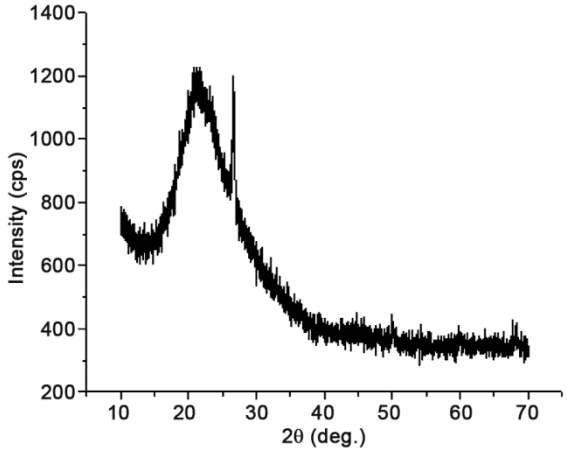

Fig. 6 — XRD pattern of CdS nanoparticles in SiO_2 sol-gel at 1000 °C.

of the CdS nanoparticles is estimated using Scherrer's formula:

$$d = \frac{0.9\lambda}{\beta Cos\theta}. \quad \ldots (3)$$

Where, λ is the wavelength of the X-ray and β is the half width of the diffraction peak and θ is the angle. The size of the CdS nanoparticles is calculated to be 9.65 nm. Though the validity of using Scherrer formula to estimate crystallite size is debatable[25-27] the result obtained is comparable to that observed from the TEM image (Fig. 7) which shows clusters of more or less spherically shaped CdS nanoparticles.

4.4 Optical properties and Judd-Ofelt analysis

The radiative and non-radiative properties of lanthanide ions have been widely reported. By Judd-Ofelt (J-O) theory, the analysis of the radiative transition in the 4f states of Sm^{3+} is performed[28, 29]. According to J-O theory, the calculated oscillator strength (f_{cal}) of the electric dipole transition between two states $|\ l^N SLJ > \rightarrow |\ l^N S'L'J' >$ can be expressed as:

$$f_{cal}^{ed} = \frac{8\pi^2 mc\bar{\nu}(n^2+2)^2}{3h(2J+1)9n} \sum_{\lambda=2,4,6} \Omega_\lambda \left|\langle l^N SLJ \| U^{(\lambda)} \| l^N S'L'J' \rangle\right|^2 \quad \ldots (4)$$

Where, m is the mass of electron, c is the velocity of light, h is Planck's constant, J is the total angular momentum of the initial state, n is the refractive index, Ω_λ are the J-O intensity parameters and $\|U^{(\lambda)}\|$ are the reduced matrix elements evaluated in the intermediate coupling approximation for transition $|l^N SLJ > \rightarrow |l^N S'L'J' >$ at energy $\bar{\nu}$ expressed in cm^{-1}. The reduced matrix elements $\| U^{\lambda}\|$ are known to be relatively host independent, so the values obtained by Carnall *et al.*[30] are used in the calculations.

The experimental oscillator strengths for transitions from the ground state to the excited states are determined from the absorption spectrum, using the following relation:

$$f_{exp} = 4.319 \times 10^{-9} \int \varepsilon(\bar{\nu})\, d\nu \quad \ldots (5)$$

Where, $\varepsilon(\bar{\nu})$ is the molar absorptivity at energy $(\bar{\nu})$ cm^{-1}. The Judd Ofelt intensity parameters are evaluated using least square fitting and the oscillator strengths obtained from Eq. (5) which is experimentally determined values co-related with the theoretical expression given in Eq. (4). The J-O intensity parameters along with the experimental and calculated oscillator strengths of 7 mol % Sm, 1 mol % CdS doped sample heated to 110 °C and the refractive index of glass sample as n=1.54 is given in Table 1.

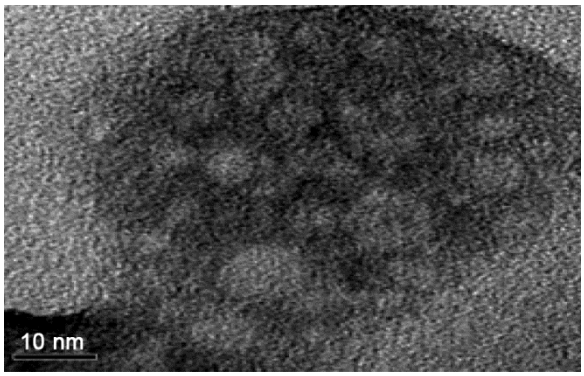

Fig. 7 —TEM image of CdS nanoparticle.

Table1 — Oscillator strengths and J-O intensity parameters for 7mol% Sm, 1mol% CdS doped sample.

Transition $^6H_{5/2}\rightarrow$	Energy (cm^{-1})	f_{exp} ($\times10^{-6}$)	f_{cal} ($\times10^{-6}$)
$^4D_{7/2}$	28901	0.267	0.397
$^4D_{3/2}$	27624	0.595	0.359
$^6P_{7/2}$	26666	0.805	0.743
$^6P_{3/2}$	24813	2.048	2.091
$^4P_{5/2}$	24038	0.337	0.316
$^4I_{13/2}$	21551	0.244	0.209
$^4I_{9/2}$	20920	0.214	0.228

Ω_2=18.508 $\times10^{-20}$$cm^2$, Ω_4=2.007$\times10^{-20}$ cm^2, Ω_6=1.445$\times10^{-20}$ cm^2 and $\Omega_4/\ \Omega_6$= 1.39

The J-O intensity parameters are found by comparing experimentally and theoretically calculated oscillator strengths, but in our present studies have found some trend that relates the parameters to the local environment of the Sm^{3+} ions. From Table 1 it is found that J-O parameters have the following trends $\Omega_2 > \Omega_4 > \Omega_6$. The large value of Ω_2 indicates the presence of covalent bonding between the rare earth ions and glass host.

The J-O parameter Ω_2 is very sensitive to the structure and it is associated with the symmetry and covalency of lanthanide sides. On the other hand Ω_4 and Ω_6 values show the viscosity and dielectric of the media and also affected by the vibronic transition of the rare earth ions bond to the ligand atoms and also related to the rigidity of the host medium in which the ions are situated, these two parameters are structure dependent parameters. J-O intensity parameters can be used to calculate the spectroscopic quality factor (SQF= $\frac{\Omega_4}{\Omega_6}$), the SQF is the deciding factor for the

luminescence transition and quality of the materials. The SQF is critically important for the stimulated emission for the laser active medium. It is used to characterize the quality of the prepared glasses[9,31,32]. Ω_4 parameters are correlated with symmetry and long range effect which is due to hydrogen bond from water molecule and Ω_6 parameters can be correlated with the rigidity of the system[33,34]. In our present studies SQF is 1.39 which indicates that the silica glasses are fairly rigid. In the previous studies the SQF of borate glass[34] is 1.71. The J-O parameters and SQF of Sm^{3+} doped glass system are presented in Table 2. The magnitude of $\frac{\Omega_4}{\Omega_6}$ indicates the optimum features among the prepared glasses.

4.5 Radiative properties

With the help of three J-O parameters we can calculate the radiative parameters. The spontaneous electric dipole transition probability between the states $|l^N SLJ>$ and $|l^N S'L'J'>$ is given as:

$$A_{ed}(SLJ, S'L'J') = \frac{16\pi^3 e^2}{3h\varepsilon_0 \bar{\lambda}^3 (2J+1)} \frac{n(n^2+2)^2}{9} \sum_{\lambda=2,4,6} \Omega_\lambda \left|\langle l^N SLJ \| U^{(\lambda)} \| l^N S'L'J' \rangle\right|^2 \quad \ldots (6)$$

Where, $\bar{\lambda}$ is the average wavelength of transition. The fluorescence branching ratio can be calculated from:

$$\beta(SLJ, S'L'J') = \frac{A(SLJ, S'L'J')}{\sum_{S',L',J'} A(SLJ, S'L'J')} \quad \ldots (7)$$

Where, the denominators are for all the transitions from the excited states $|l^N SLJ>$ to the lower energy states. The radiative lifetime of an excited state $l^N SLJ>$ is given as:

$$\tau(SLJ) = \left(\sum_{S',L',J'} A(SLJ, S'L'J')\right)^{-1} \quad \ldots (8)$$

These equations are used to calculate the radiative parameters of the glass sample which is shown in Table 3.

For laser applications an important parameter which determines the potential of a material is the stimulated emission cross-section. The stimulated emission cross-section σ_{emi} can be determined from the emission spectrum and the calculated emission probability using the relation[38]:

$$\sigma_{emi} = \frac{{\lambda_p}^4}{8\pi c n^2 \Delta\lambda_{eff}} A_{ed} \quad \ldots (9)$$

Where, λ_p is the peak emission wavelength, $\Delta\lambda_{eff} = \frac{\int I(\lambda) d\lambda}{I_{max}}$ is the effective line width, n is the refractive index and A_{ed} is the emission probability for the particular transition obtained from Table 3. Table 4 shows that the sample with lower ratio

Table 2 — Judd-Ofelt intensity parameters and spectroscopic quality factor (SQF = $\frac{\Omega_4}{\Omega_6}$) of varying Sm^{3+} concentration in the different glass matrix.

Glass	Intensity parameters Ω_λ ($\times 10^{-20}$ cm^2)			Quality Factor ($\frac{\Omega_4}{\Omega_6}$)	Trends of Ω_λ
	Ω_2	Ω_4	Ω_6		
Silica Glass (Present Work)	18.508	2.007	1.445	1.39	$\Omega_2 > \Omega_4 > \Omega_6$
Sodium-tellurite glasses, TNS4 (Ref. [9])	0.802	0.719	0.449	1.61	$\Omega_2 > \Omega_4 > \Omega_6$
Fluoro-tellurite (Ref. [35])	4.94	3.15	1.75	1.8	$\Omega_2 > \Omega_4 > \Omega_6$
Tungsten tellurite (Ref. [36])	6.68	3.78	1.86	2.03	$\Omega_2 > \Omega_4 > \Omega_6$
Borate glass (Ref. [34], [37])	6.36	6.02	3.51	1.71	$\Omega_2 > \Omega_4 > \Omega_6$
20ZnO-10Li_2O-10Na_2O-60P_2O_5 (Ref.[8])	1.07	1.457	0.8402	1.7341	$\Omega_4 > \Omega_2 > \Omega_6$

Table 3 — Spontaneous emission probabilities, radiative lifetimes and branching ratios calculated for Sm^{3+} using J-O intensity parameters Ω_2=18.508×10^{-20}cm^2, Ω_4=2.007×10^{-20} cm^2 and Ω_6=1.445×10^{-20} cm^2

Transition $^4G_{5/2} \rightarrow$	Average Energy (cm^{-1})	A_{ed} (s^{-1})	β (%)	τ (μs)
$^6H_{5/2}$	17930	4.55	1.02	2259.94
$^6H_{7/2}$	16896	50.29	11.36	
$^6H_{9/2}$	15690	292.44	66.08	
$^6H_{11/2}$	14364	13.56	3.06	
$^6H_{13/2}$	12959	1.73	0.39	
$^6F_{3/2}$	11394	10.75	2.43	
$^6F_{5/2}$	10890	59.69	13.48	
$^6F_{7/2}$	10022	1.25	0.28	
$^6F_{9/2}$	8842	8.23	1.86	

Table 4 — The stimulated emission cross-section σ_{emi} calculated for Sm^{3+} using J-O intensity parameters Ω_2=18.508×10^{-20}cm^2, Ω_4=2.007×10^{-20} cm^2 and Ω_6=1.445×10^{-20} cm^2

Transition $^4G_{5/2}\rightarrow$	Average Energy (cm^{-1})	λ_p(nm)	$\Delta\lambda_{eff}$(nm)	σ_{emi} (×10^{-22}cm^2)
$^6H_{5/2}$	17930	562	6.45	0.39
$^6H_{7/2}$	16896	596	11.33	3.13
$^6H_{9/2}$	15690	644	13.75	20.46
$^6H_{11/2}$	14364	705	17.31	1.08

Sm/CdS has higher σ_{emi} value as a result of narrower effective line width.

5 Conclusions

Sol-gel process has been employed to prepare Sm^{3+} ions along with CdS crystallites doped in silica glasses. The size of the CdS crystallites has been estimated by effective mass approximation and from the XRD pattern using Scherrer formula. From the optical absorption and PL spectra, the three Judd-Ofelt intensity parameters, spontaneous emission probabilities, radiative lifetime and stimulated emission cross-section of Sm^{3+} ions doped in CdS and Silica glasses are determined. The observed trend in the variation of the J-O parameter was $\Omega_2 > \Omega_4 > \Omega_6$. The large value of Ω_2 indicates the presence of covalent bonding between the rare earth ions and glass host. On the other hand Ω_4 and Ω_6 values show the viscosity and dielectric nature of the media and also affected by the vibronic transition of the rare earth ions bond to the ligand atoms. Strong emissions in the visible region were observed under UV excitation.

Acknowledgement

Md Uzair Khan is thankful to university Grants Commission, India for UGC-MZU (Non-NET) fellowship, for financial support with Award letter No.2-5/MZU (Acad)/16/685. Authors wish to thank Department of Chemistry, Mizoram University for use of FTIR measurement equipment.

References

1 Qiao Y, Li S, Liu W, Ran M, Lu H & Yang Y, *Nanomaterials*, 8 (2018) 43.
2 Rai S, Bokatial L & Dihingia P J, *J Lumin*, 131 (2011) 978.
3 Fanai A L, Khan U & Rai S, *J Non-Cryst Solids*, 503 (2019) 89.
4 Chakraborti S, Sahu J, Chakraborty M & Acharya H N, *J Non-Cryst Solids*, 180 (1994) 96.
5 Rai S & Fanai A L, *J Lumin*, 170 (2016) 325.
6 Rai S & Fanai A L, *J Non-Cryst Solids*, 449 (2016) 113.
7 Donato K Z, Matˇejka L, Mauler R S & Donato R K, *Colloid Interf*, 1 (2017) 5.
8 Ramteke D D, Balakrishna A, Kumar V & Swart H C, *Opt Mater*, 64 (2017) 171.
9 Mawlud S Q, Ameen M M, Sahar M R, Mahraz Z A S & Ahmed K F, *Opt Mater*, 69 (2017) 318.
10 Zhang X, Wu D & Geng H, *Crystals*, 7 (2017) 307.
11 Huynh W U, Dittmer J J & Alivisatos A P, *Science*, 295 (2002) 2425.
12 Yang F, Tian X, Zhang K, Zhang X & Liu L, *ECS J Solid State Sci Technol*, 7 (2018) 311.
13 Wild D S, Shahmoon E, Yelin S F & Lukin M D, *Phys Rev Lett*, 121 (2018) 123606.
14 Fahad H M, Shiraki H, Amani M, Zhang C, Hebbar V S, Gao W, Ota H, Hettick M, Kiriya D, Chen Y Z, Chueh Y L & Javey A, *Sci Adv*, 3 (2017) 1.
15 Bhambhani P & Alvi P A, *J Optoelectronics Engineering*, 4 (2016) 11.
16 Yang X, Shan C X, Ni P N, Jiang M M, Chen A Q, Zhu H, Zang J H, Lub Y J & Shen D Z, *Nanoscale*, 10 (2018) 9602.
17 Cao H, Wang G, Zhang S, Zhang X & Rabinovich D, *Inorg Chem*, 45(13) (2006) 5103.
18 Singh V & Chauhan P, *Chalcogenide Lett*, 6 (2009) 421.
19 Rajeshwar K, de Tacconi N R & Chenthamarakshan C R, *Chem Mater*, 13 (2001) 2765.
20 Hayakawa T, Selvan S T & Nogami M, *J Sol Sci Technol*, 19 (2000) 779.
21 Hayakawa T, Selvan S T & Nogami M, *J Lumin*, 87 (2000) 532.
22 Reisfeld R, Gaft M, Saridarov T, Panczer G & Zelner M, *Mater Lett*, 45 (2000) 154.
23 Rai S, Bokatial L & Dihingia P J, *J Lumin*, 131 (2011) 978.
24 Brus L E, *J Chem Phys*, 80 (1984) 4403.
25 Scardi P, Leoni M & Delhez R, *Appl Cryst*, 37 (2004) 381.
26 Detlef M S, *J Appl Cryst*, 42 (2009) 1030.
27 Pawel E T, *Phase Trans,* 86 (2013) 260.
28 Judd B R, *Phys Rev*, 127 (1962) 750.
29 Ofelt G S, *J Chem Phys*, 37 (1962) 511.
30 Carnall W T, Fields P R & Rajnak K, *J Chem Phys*, 49 (1968) 10.
31 Nii H, Ozaki K, Herren M & Morita M, *J Lumin*, 76 (1998) 116.
32 Praveena R, Venkatramu V, Babu P & Jayasankar C K, *Phys B Condens Matter*, 403 (2008) 3527.
33 Lakshminarayana G, Yang R, Qiu J R, Brik M G, Kumar G A & Kityk I V, *J Phys D: Appl Phys*, 42 (2009) 015414.
34 Agarwal A, Pal I, Sanghi S & Aggarwal M P, *Opt Mater*, 32 (2009) 339.
35 Ghosh A & Debnath R, *Opt Mater*, 31 (2009) 604.
36 Venkatramu V, Babu P, Jayasankar C K, Tröster Th, Sievers W & Wortmann G, *Opt Mater*, 29 (2007) 1429.
37 Boehm L, Reisfeld R & Spector N, *J Solid State Chem*, 28 (1979) 75.
38 Jacobs R R & Weber M J, *IEEE J Quantum Electron*, 12 (1976) 102.